Environmental Fluid Mechanics (2023) 23:489–510
https://doi.org/10.1007/s10652-023-09914-4

ORIGINAL ARTICLE

Fog-laden density staircases in the marine atmospheric boundary layer

Harindra J. S. Fernando[1,2] · Sen Wang[1] · Kelly Y. Huang[1] · Ed Creegan[1,3]

Received: 28 October 2022 / Accepted: 15 February 2023 / Published online: 12 March 2023

Abstract
The formation of a layered structure in the form of vertically separated density steps (staircases) in stably stratified fluids has been reported in many laboratory and oceanic studies as well as in the terrestrial atmospheric boundary layer (ABL) to a lesser extent, with attribution to different dynamical mechanisms. This paper presents observations of layered structures in fog-laden marine ABL, where both fog and density steps appear almost simultaneously following a turbulent mixing event under nocturnal conditions. The observations were made during the C-FOG (2018) field campaign aboard a research vessel using rawinsonde launches, aided by a suite of supporting onboard instruments. This is a case of great practical interest because of the impediment by fog-laden staircases to optical and near-infrared wave propagation in the ABL due to enhanced beam jitter by density steps and beam attenuation by fog. A new mechanism is proposed to explain the genesis of density layering, wherein steps appear when fluid parcels with significant buoyancy differences (Δb) osculate in regions of weak turbulence (local length and velocity scales, L_H and u_H, respectively) devoid of adequate inertial forces ($\sim u_H^2/L_H$) to cause fluid parcels to stir past each other. This is expressed in terms of a local bulk Richardson number criterion $Ri = \Delta b L_H/u_H^2 > Ri_c$, where Ri_c is a critical value. A simple laboratory experiment with an idealized (three layer) density stratification and a known turbulence source (oscillating grid) was performed to demonstrate the proposed mechanism, and through a combination of measurements and modeling it was found $Ri_c \approx 1.5$. The proposed criterion was consistent with C-FOG field observations as well as representative previous layering observations in the atmosphere and ocean due to localized turbulence mixing events caused by Kelvin–Helmholtz billowing.

Keywords Stratified flows · Marine atmospheric boundary layer · Fog · Density steps

✉ Kelly Y. Huang
yhuang28@nd.edu

[1] Department of Civil and Environmental Engineering and Earth Sciences, University of Notre Dame, Notre Dame, IN, USA

[2] Department of Aerospace and Mechanical Engineering, University of Notre Dame, Notre Dame, IN, USA

[3] Army Research Laboratory, White Sands Missile Range, NM 88002, USA

1 Introduction

This paper concerns the formation of approximately well mixed [turbulent] air layers vertically separated by thin, sharp density jumps known as density staircases in the lower atmospheric boundary layer (ABL) under calm and stably stratified conditions [1, 2]. These density jumps or interfaces are sufficiently strong to impede effective turbulent mixing across them, and turbulence within these interfaces are damped (non-Kolmogorov), intermittent and of very small-scale [3], and possibly produced by interfacial wave breaking [4]. While the temperature (density) structure in ABL is important and has been studied in the context of a variety of applications such as pollution dispersion and temperature spikes in cold-air pooled valleys, an interesting set of applications has come to light in view of newer technologies related to Free-Scale Optical (FSO) transmission and High Energy Laser (HEL) defense systems. In the former, communications between local signal recipients and a central fiber-optics communication hub are effectuated using FSO links to avoid infrastructure modification (e.g., digging and burying of cables, hardware installations) in congested areas. To obtain high data rates, optical wave lengths (0.4–0.8 μm) are used in FSO, referred to as optical local area networks (LAN) or optical wireless. In HEL applications, focused beams with tens and hundreds of kW power at optical or near infrared (IR, 1–1.5 μm) wavelengths are used to deliver heat and eliminate enemy targets. HELs are particularly important in staving off proliferating threats from a swarm of small, unmanned aircraft systems (UAS), for which large kinetic defense systems are ineffective. Maintaining focus of the beam within the same area of the target for several seconds is necessary in this case, which is hampered by beam wander, scatter, and absorption by environmental effects. The most significant bane is from refractive index variations that optically distort the beam. For visible and low IR radiation, the refractive index of air is directly related to density via the Gladstone-Dale constant [5]. In turn, the air density is strongly sensitive to temperature and humidity variations along the beam propagation path [6].

If the refractive index is nonuniform over the beam diameter, the distortion of a monochromatic wave front is categorized into mean and tip/tilt components as well as higher order disturbances. The tip/tilt characterizes the bending of the beam, which produces anomalous electromagnetic (EM) beam paths that refract the beam toward the ground producing EM ducts. The dynamic component of tip/tilt produces beam 'jitter.' EM ducting confuses detection devices such as radars by causing 'ghost' images and shadow zones (i.e., radar holes). Conversely, the higher order disturbances diffract and spread the beam energy in the far field. The tip/tilt is contributed by turbulence structures larger than the beam diameter whereas higher-order disturbances by those smaller than the beam diameter. The overall refractive index fluctuations in general are known as optical turbulence. As such, thin density steps in staircases have pronounced implications on optical turbulence in the ABL, considering that typical transmitting beam diameter is ~ (1–2) m that expands along the beam. For thin density stratified layers with intermittent turbulence patches embedded, both large- and small-scale turbulence structures are all within the beam diameter, thus affecting the propagation drastically.

An additional difficulty arises when water vapor is present, whence the refractive index is frequency dependent, with lower frequencies being affected more compared to optical frequencies. When fog is formed with suspended water droplets under saturated conditions, however, optical wavelengths are also sapped, and molecular absorption becomes important for wavelengths shorter than 50 μm [7]. Fog typically has a bimodal particle diameter distribution with peaks in the ranges of 1–2 μm and 15–25 μm, with the former interfering with optical/

near-IR beams to reduce visibility. The American Meteorological Society glossary defines fog as the condition where the ground level visibility (*vis*) is less than 1 km causing severe disruptions in transportation, agriculture, and human health sectors [8].

This paper addresses the compelling case of density layering in stable marine ABL accompanied by fog, which provides severe barriers for optical propagation in the ABL. To our knowledge, this is the first paper that delves into such an ABL configuration, enabled by observations made during the Coastal-Fog (C-FOG) field experiment discussed in Fernando et al. [9], Dorman et al. [10] and Wang et al. [11]. The observational platforms deployed during C-FOG for visibility, fog, turbulence, and vertical profiling are discussed in Sect. 2, followed by observations of a density-layered fog event in the ABL presented in Sect. 3. A brief review of previous research on layered structure formation is given in Sect. 4, and a new phenomenological mechanism for step genesis is presented in Sect. 5. Since fog acts as a passive scalar, the proposed mechanism is expected to hold both in the presence and absence of fog. A laboratory experiment to illustrate the proposed mechanism is given in Sect. 6 and an analysis of flow evolution and turbulent parameters in Sect. 7 and Sect. 8. Experimental observations are described in Sect. 9, followed by concluding remarks and a discussion in Sect. 10.

2 Observational platforms

The C-FOG field program was conducted during 01 September to 08 October 2018 in the east coast and coastal waters of Newfoundland and Nova Scotia, Canada to study the formation, maturation, and dissipation (i.e., life cycle) of coastal fog. This comprehensive study consists of three field stations along the east coast of Avalon Peninsula, Newfoundland and in Nova Scotia. As part of the project, the research vessel (R/V) Hugh R. Sharp conducted measurements in Avalon coastal waters, and the array of instruments deployed on R/V Sharp is shown in Fig. 1a with a detailed description given in Fernando et al. [9]. The instruments exclusively employed for this study are given in Table 1 and depicted in Fig. 1b–e. During the field campaign, three fog episodes were encountered by the ship (although much more was anticipated), which are designated as Ship Intense Operational Periods: SIOP-1 (1700 UTC 12 Sep to 0700 UTC 13 Sep), SIOP-2 (0900 -1600 UTC 28 September) and SIOP-3 (2000 UTC to 2230 UTC 04 October). The ABL measurements in this paper concern SIOP-1, which was the only SIOP identified as a 'mixing fog' event caused by vertical mixing between two or more airmasses in the lower ABL [9]. The ship location during this episode is given in Fig. 1f, with the presence of fog identified by darker colors when visibility < 1 km. The other two events were dominated by stratus cloud lowering events [9], and hence will not be discussed here nor did they exhibit any layering in the lower ABL. Observed fog and microphysical properties of SIOP-1 are described by Wang et al. [11] and SIOP-2 and SIOP-3 by Wagh et al. [12].

3 Layering observations

Figure 2a shows a sequence of rawinsonde profiles taken from R/V Sharp during SIOP-1 from 17:21 UTC on 12 September to 08:14 UTC on 13 September 2018, with the ordinate representing height z above sea level (asl). The wind vectors (directional barbs), air temperature T_{air}, dew point T_d and equivalent potential temperature θ_E are shown, where θ_E is a surrogate for air density when the liquid water content in the air is small, and is obtained by first computing the potential temperature at lifting condensation level (LCL)

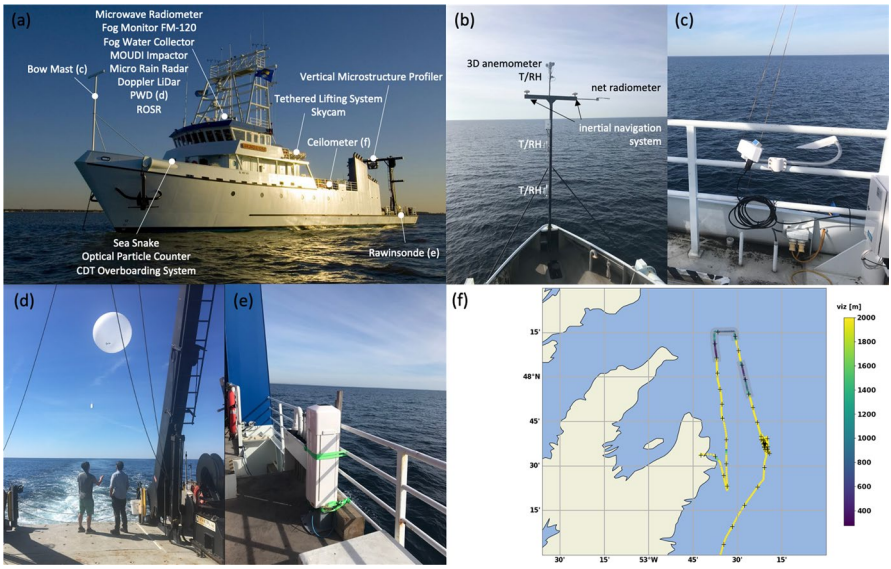

Fig. 1 **a** Array of instruments used in the R/V (see Fernando et al. [9] for details), with specific instruments used for the present study—bow mast (**b**), PWD (**c**), Rawinsonde system for vertical profiling (**d**), and CL31 ceilometer (**e**) (See Table 1 for details). **f** Ship Track during SIOP-1, with the visibility (*vis*) color coded in the side bar, with $vis < 1$ km are fog periods

and subsequently accounting for moisture content [13, 14]. Figure 2b shows the gradient Richardson number Ri_g calculated with horizontal velocities, virtual temperature, and potential temperature by averaging over 15 m, showing local peaks in the density steps. Figure 2c shows the standard ceilometer backscatter, wherein the lowest strong backscatter level indicates the cloud base closest to the ground. While the presence of other backscatter layers indicates cloud layers aloft, the attenuation of ceilometer IR light at the lowest cloud base may obscure the presence of backscatter layers aloft, let alone their details. Figure 2d shows turbulence parameters, turbulent kinetic energy (TKE) and its dissipation measured using the bow-mast sonic anemometer. The dissipation rate of TKE was retrieved using the inertial-subrange method, and the visibility (*vis*) was measured by PWD-22 at ~ 9.1 m asl. The appearance of fog is synonymous with $vis < 1$ km.

At 17:21 UTC, the air column is saturated from about 100 m to 1 km, with the lowest cloud base at ~ 100 m, as indicated by strong ceilometer backscatter intensity at that height (Fig. 2c.i). The wind speed below ~ 400 m is ~ 30 knots and southerly (from the south), presumably consisting of humid and warm advected air over warm ocean (Fig. 2a.i). The air column is generally stably stratified (note the θ_E profile), but below 100 m or so it is strongly stratified and unsaturated ($RH \sim 99\%$). At 20:15 UTC (Fig. 2a.ii), an unsaturated ($RH < 96\%$) and warmer airmass arriving from the west (westerly) at 15 knots is located above 600 m with strong shear between saturated southerly and unsaturated westerly layers indicating a region of strong mixing, as evident from an θ_E inversion and $Ri_g < 0$ just below 600 m (Fig. 2b.ii). Above this level is a stable layer with stable inversion. Evolution from 17:21 to 20:15 UTC is eventful, consisting of first a general decrease of TKE at the surface level and then sustained turbulent levels (Fig. 2d.i to ii) along with chaotic breakdown of the cloud layer aloft at ~ 250 m (Fig. 2c.i to ii). Stable stratification prevails, causing the decay of TKE thereafter. At the third rawinsonde time of 23:11 UTC (Fig. 2a.

Table 1 Instruments used for the study reported in this paper (further information on instruments and their resolution and accuracies are given in Fernando et al. [9])

Instrument	Measurement	Information
Bow mast of the ship (height of 14 m from the deck)	Three levels of HMP155 T/RH probes (at 7, 9, and 12.5 m); CSI IRGASON at 12.5 m; K&Z CNR4 net radiometer at 11.5 m; VectorNav VN100 IMU and Trimble BX982 Dual-GNSS receiver for motion correction	HMP155—temperature *T*, relative humidity *RH* K&Z CNR4 net radiometer—incoming and outgoing radiation
Vaisala RS41-SGP radiosonde launches and Digi-CORA Sounding System MW41	Rawinsondes were released at varying time intervals (1–3 h) during SIOPs	Typical releases were at 0000 and 1200 UTC, with increased frequency during SIOPs
Vaisala CL31 Ceilometer	Cloud/fog base height and aerosol backscattering, typically 3-cloud layers	Cloud-/fog-base height and aerosol backscattering, three cloud layers
PWD22 visibility sensor	Continuous operation, fixed to R/V guardrails	Visibility, precipitation

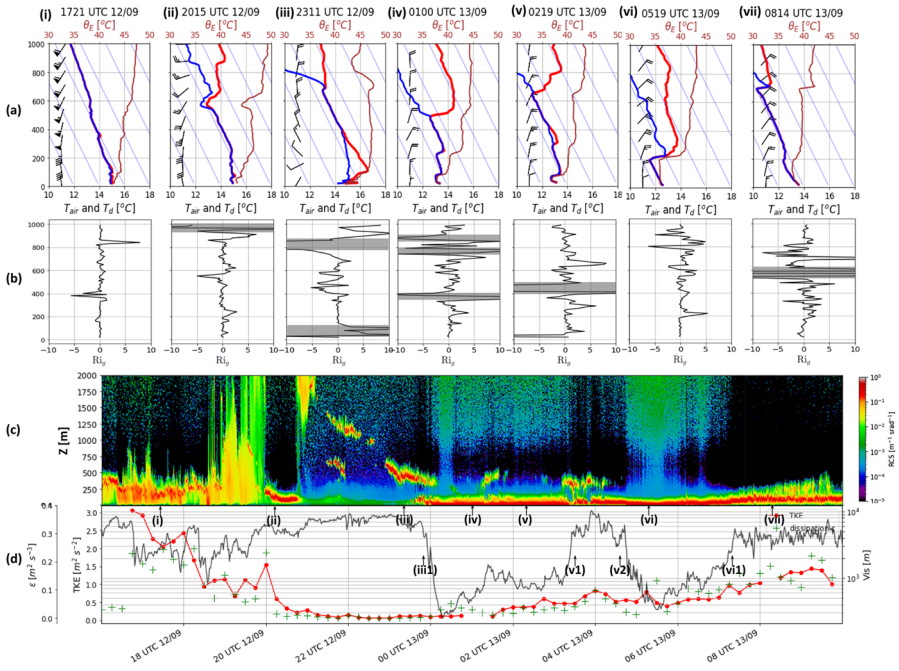

Fig. 2 **a** Radiosonde profiles of air temperature (red), dew point (blue) and equivalent potential temperature (dark red) below 1000 m during SIOP-1. Wind barbs: half line means 2 ms^{-1}, full line means 4 ms^{-1}, and one flag means 20 ms^{-1} of horizontal wind speed. **b** Gradient Richardson number based on 10 m intervals for the lower 1 km (gray semi-transparent bars marks the region of near-zero wind shear, which resulted in unrealistically large Richardson numbers). **c** Ceilometer backscatter profile during SIOP-1. **d** TKE and its rate of dissipation (ϵ) as measured using a sonic anemometer at ~ 12.5 m asl. Visibility measured by PWD-22 at ~ 9.1 m asl is plotted as a dark gray line. Note that the tick marks (arrows) common to **c**, **d** correspond to the timestamps of rawinsonde launches in **a**

iii), a saturated layer exists over 400 to 600 m, but high CL31 backscatter is confined to the lower edge of the saturated layer because of signal blanking above. Thence weak winds (~ 5 knots) prevail near the ground with northerly winds aloft, and there is an unsaturated layer between a nearly saturated ground layer and a saturated layer at ~ 400 m. The first 100 m is very stable (Fig. 2a.iii), with a weakly stratified layer aloft.

The major layering episode occurs between 23:11 and 01:00 UTC (Fig. 2a.iii to iv)—possibly around 23:45 UTC (Fig. 2d.iii) where the visibility drops from ~ 7 km to less than 300 m over a few minutes—where a fog layer with strong CL31 backscatter appeared near the ground (Fig. 2d.iii1) with possible overlying saturated layers which are masked by the ground fog layer. Turbulence intensity continues to remain low at the ground level (Fig. 2d), and the 01:00 UTC rawinsonde vividly registers the water–vapor saturated density (or θ_E) step structure up to about 500 m (Fig. 2a.iv). Density steps at ~ 100 m, 200 m and 400 m are all quite stable with high Ri_g, evident from Fig. 2b.iv. The presence of fog at ground level (Fig. 2d) and aloft (Fig. 2c) are evident. The northerly winds prevail up to 1 km with little shear, and hence meager turbulent mixing. Until the next rawinsonde at 02:19 UTC (Fig. 2a.v), the evolution is slower, with density layers slowly migrating possibly due to differential turbulence levels in the homogeneous layers [16]. The visibility remains low in the fog regime, with some slow modulations.

Between the 02:19 and 05:19 UTC rawinsondes, there has been a turbulence generating event at v1 (Fig. 2c, d, v to vi), leading to breakup of the fog layer and increased visibility. The event is followed by a low level cloud and reestablishment of a fog layer (v2) just before the 05:19 UTC sounding (Fig. 2d.vi), whence the lower layer appears to be well mixed (Fig. 2a.vi), saturated and foggy up to 200 m (Fig. 2c), and have elevated turbulent levels (higher TKE and dissipation) with low northerly winds ~ 5 knots in the lower layer topped by a highly stable density interface at 200 m. Above 200 m, drying can be seen with northeasterly winds. Increase of turbulence levels and lifting of fog starts at vi1, with marked increase in surface visibility at the time of the next rawinsonde at 08:14 UTC (Fig. 2a.vii). Increase of turbulence at vi1 is consistent with the slightly mixed air column up to 650 m, topped by a strong density interface. The lower layer (~ 100 m) has strong turbulence levels and high visibility ($Ri_g \leq 0$) notwithstanding near saturation conditions, aloft of which seems to have a low-level cloud with fluctuating Ri_g and backscatter intensities penetrating to hundreds of meters. In all, the lowest surface visibility is encountered during the presence of a density step structure.

4 Summary of previous work on density step genesis

Observations made in stably stratified oceans and in the atmosphere [17–20] have provided evidence for staircases characterized by density steps separated by significantly mixed turbulent layers undergoing mixing (or mixing layers). Laboratory [19, 21] and modeling [22, 23] studies also abound. In the ocean, when staircases are of meter scale, the layered structure is considered as a microstructure that takes the form of either jagged density profiles [24] or density steps [17]. The jagged profiles can be attributed to displacement of fluid elements of varying densities from a stable profile due to background turbulence or to a recently defunct turbulent event in the probing area that has not had time to revert its perturbed density field to a stable state. Conversely, different mechanisms may dominate the formation of distinct step microstructures, and some possibilities are: (a) the presence of a continuously breaking internal wave that leaves a trail of locally mixed fluid as it travels through the fluid [25, 26]; (b) the presence of double-diffusive instabilities in the form of salt-fingering or diffusive interfaces [27, 28]; (c) instabilities due to sidewall heating of salt-stratified fluids [29]; (d) collapse of locally mixed fluid masses due to boundary mixing, forming a series of intrusions into the stratified layer [30]; (e) thermohaline shear instability [31], and (f) the decrease of [density] eddy diffusivity in stratified turbulent flows with the increase of buoyancy gradient (in such a way that the increase of buoyancy flux due to the increase of buoyancy gradient is compensated by a corresponding reduction in eddy diffusivity [32–35]). These mechanisms are based on formal theoretical analyses or phenomenological descriptions based on the concept of eddy diffusivity and its dependence on the local Richardson number [36], although a unified theoretical explanation for this reduction is still lacking. It is noteworthy that the above descriptions have been developed for ocean and boundary-dominated flows. Below we discuss an alternative mechanism for the formation of density steps in stratified turbulent fluids developed in the context of layering in stable ABL, oceanic thermocline or even stratified upper levels of the atmosphere.

5 A phenomenological mechanism for step formation

Figure 3 schematizes a plausible step formation mechanism when a stable density-stratified region (represented by a positive θ_E gradient) is subjected to a localized turbulence event initiated at time $t = 0$. The characteristic *rms* velocity and the integral length scales of turbulence are u_H and L_H, respectively. Turbulence causes eddying motions of fluid parcels with different densities, taking lighter parcels (e.g., B) downward and heavier parcels (e.g., A) upward, leading to a jagged temperature (density) profile [Fig. 3a, b (i,ii)] mostly without changing the density of individual parcels—the process of turbulent "stirring". Soon, the local temperature gradients amplify, and nearby fluid parcels begin to exchange heat, thus changing their temperature (densities) and smearing off small scale gradients [Fig. 3a, b (iii)]—turbulent "mixing." During the initial evolution ($t < L_H/u_H$), however, the temperature structure is dominated by stirring [37], and eddies of integral scale are responsible for transporting fluid parcels against buoyancy forces. The largest buoyancy forces are encountered by fluid parcels entrained from the edges of the turbulent patch [say A and B in Fig. 3a, b (ii–iii)], as they attempt to cross each other's territories through the central area of the turbulent patch. If the densities of fluid parcels (modified by mixing) when they meet at C are ρ'_A and ρ'_B, B fluid parcels experience a positive buoyancy of $-\left(\rho'_B - \rho'_A\right)g/\rho_0 = \Delta\rho' g/\rho_0 = \Delta b(> 0)$ where $\Delta\rho' = -\left(\rho'_B - \rho'_A\right)$ and $\rho_0 \approx \left(\rho_1 + \rho_2\right)/2$, whereas A parcels encounter a similar but negative buoyancy force. If the characteristic inertial forces of fluid parcels (u_H^2/L_H) can overcome the retarding buoyancy forces (Δb) at C, they may penetrate and stir the entire turbulent fluid column [Fig. 3a (iv)], i.e., $\Delta b < u_H^2/L$ or $Ri = \Delta b l_H/u_H^2 < 1$, where Ri is a bulk Richardson number. This condition can be written as $Ri < Ri_c$, where Ri_c is a critical bulk Richardson number below which

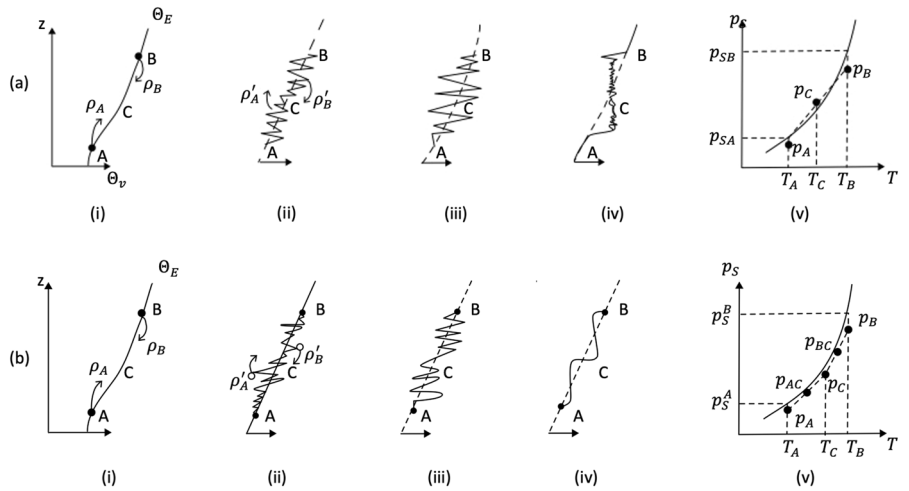

Fig. 3 Schematics of equivalent potential temperature [or density] profile sequence (i)–(iv) illustrating mixing in a stably stratified fluid by a localized turbulence event: **a** without discernible, semi-persistent density step formation, and **b** with formation of a density step. (v) shows the saturation water vapor pressure p_s versus temperature T diagram indicating how water vapor pressure of fluid parcels change during mixing. In **a** (v), unsaturated air parcels A and B mix to form a mixed parcel C that is saturated with possible fog. In **b** (v), air parcels at B and C mix to form the parcel BC as well as A and C to form AC, and both p_{BC} and p_{AC} are in the near saturation state that may produce fog while A, B and C are unsaturated

fluid parcels penetrate over the entire middle layer and no density step is formed [Fig. 3a (iv)]. When $Ri \geq Ri_c$ the parcels may not penetrate past each other, and a density step or layered structure is expected [Fig. 3b (iv)], with the vertical extent of overturning turbulent eddies limited by the density step. If turbulence is sustained, the regions above and below the density step will continue to undergo stirring and mixing, slowly transferring buoyancy across the interface and reducing the buoyancy jump Δb across the interface, finally breaking the step when Ri drops below Ri_c. Events of this ilk may lead to multiple turbulent layers with density steps sandwiched in between. While turbulence intensities above and below the interface in this case are the same, they may differ in real situations, whence the steps tend to migrate and possibly merge with each other [15].

Figure 3a, b (v) show how moisture may evolve during a turbulent event, in relation to observations in Sect. 2. Figure 3a (v) shows the position of A and B fluid parcels with respect to the saturation vapor pressure–temperature ($p_s - T$) curve. The vapor pressure at A (p_A) and B (p_B) are both smaller than the respective saturation pressures p_{SA} and p_{SB} at the temperature of A (T_A) and B (T_B). Given both levels are unsaturated, no fog is present. Turbulent mixing of two air masses, however, leads to a water vapor pressure of p_C (temperature T_C), which is saturated and possibly containing fog. This is a result of the nonlinear behavior of the $p_S - T$ curves that was first discussed by Taylor [38]. The case of layer formation and saturation is shown in Fig. 3b (v). Here mixing is inhibited across the step at C, but sustained mixing is present in the two surrounding turbulent layers. Although p_B, p_C and p_A are all unsaturated, mixing produces p_{BC} and p_{AC}, both of which can be saturated with possible fog. Overall, the above illustration mimics the case of Fig. 2c–d where mixing of unsaturated air masses leads to density steps in a foggy environment.

6 Laboratory demonstration

To demonstrate the viability of the proposed mechanism using a laboratory experiment, a simple variant of the flow configuration of Fig. 3 was adopted, schematized in Fig. 4a, b. This selection ameliorates practical difficulties of obtaining a controlled distribution of turbulence properties in a laboratory-simulated flow. Here a turbulent region is maintained between two density interfaces of a three-layer fluid using two oscillating grids placed symmetrically above and below the center of the stirred turbulent layer. The distance between a grid and its closest density interface was the same for both grids. Two grids were used instead of [commonly used] single grid so that the central region of the anticipated density step is devoid of direct mechanical forcing and lay in a region of nearly homogeneous turbulence, as demonstrated by Srdic et al. [39]. By changing the frequency of grid oscillations, turbulent intensity and interfacial mixing in the center area could be adjusted.

The experiments were conducted in a Plexiglas tank of square cross section 25.5×25.5 cm and height 45.5 cm, the same as in De Silva & Fernando [40, 41], where the details of construction and turbulence measurements are given. The grids were independently oscillated using speed-controlled DC motors via slider-crank mechanisms. During each experiment, the frequency of oscillation of the two grids were the same, with motor speeds maintained constant within $\pm 0.5\%$ of the mean speed. The grids were made of 0.8×0.8 cm square Plexiglas bars with a mesh size $M = 5$ cm center to center rigidly suspended horizontally within the tank by using three stainless steel rods of 0.3 cm diameter. The ends of the rods were bolted to the grid, placed symmetrically relative to its center, and the other ends were connected to a three-arm support template. Each template was

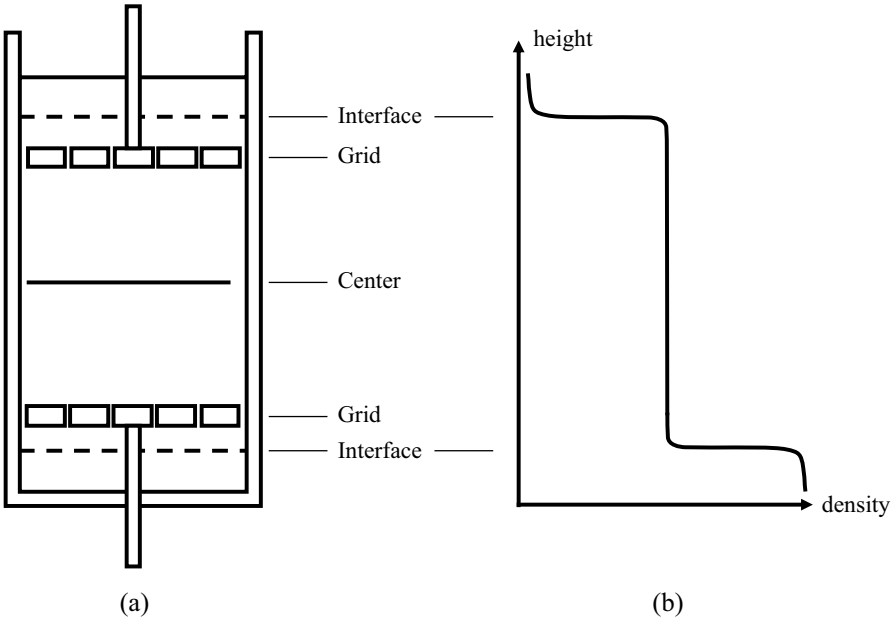

Fig. 4 A schematic of **a** the experiment set up to mimic flow configuration shown in Fig. 3; **b** the initial density (salt) profile used

driven by a single reciprocating rod, guided by a pillow block bearing. The mean positions of the bottom and top grids were at distances 12 cm and 30.6 cm, respectively from the bottom of the tank. The strokes of both grids were set to $S = 3.5$ cm. To minimize turbulence generated by connecting rods and possible secondary circulation, the motor was operated at frequencies $f < 6$ Hz, mostly at 4 and 5 Hz [42, 43].

Prior to an experiment, the tank was filled with the three-fluid system (Fig. 4b), with the density of each layer adjusted by varying the concentration of dissolved salt with the middle layer having the mean density of the top and bottom layers. Fluid of different densities were slowly fed through a capped hole at the tank bottom tank until the desired fluid heights and 3-layer stratification were reached. Given the slow speed of fluid metered through the capped hole, ensuing circulation in lifted fluid layers was weak with minimal interfacial mixing, even when the two interfaces were rising past the two [stationary] grids. The thinness of density interfaces measured prior to each experiment compared to the homogeneous layer thicknesses confirmed the lack of mixing during filling. After filling, the interfaces were located 4–6 cm above of (or below) the closest grid-reach during oscillations. The density measurements were made using a four-electrode conductivity probe (MSI Instruments) attached to a vertical traversing platform. The probe could be traversed at a preset speed of 5 cm/s, and the conductivity and potentiometer voltage of the traversing system were converted to density data using standard calibration procedures [40].

Grids were initially located at their mean positions and the initial density profile was recorded. The experiments were started by simultaneously starting the motors at time $t = 0$. The oscillating frequencies of both grids were the same, and they were set to oscillate out of phase symmetrically with respect to the center. The oscillating frequencies were recorded by electronic tachometers attached to oscillating mechanisms. The density fronts generated at the interfaces due to local turbulent mixing propagated toward the tank center

and osculated each other during which a density step was formed in some experiments whereas others show no density steps. In the former, upon continuation of turbulent forcing, buoyancy jump across the step gradually decreased, and finally the two layers merged because of breakup of the step. The evolution of density profiles was monitored by traversing the conductivity probe with 0.5–1 min time separations. The horizontal location of the vertically penetrating probe was ~ 9 cm from the center of the tank along a diagonal, in the center of a grid element, to reduce the direct grid influence. In addition, a shadowgraph was used to qualitatively observe the formation of density step structures. Although only a single horizontal location was measured, from the shadowgraph it appeared to be a good indicator of the averaged position of the newly formed interface that spanned the entire tank horizontally. An experiment typically lasted for about 20–30 min.

7 Analysis of flow evolution

A schematic of the flow evolution is shown in Fig. 5 with nomenclature used, where two density interfaces at time $t = 0$ are located above and below a distance h from the mean position of [oscillating] grids. The density and buoyancy of the upper layer are ρ_u^0 and b_u^0, respectively, with $b_u^0 = -g(\rho_u^0 - \rho_0)/\rho_0$, and the middle layer density is approximately $\rho_{0=}\left(\rho_u^0 + \rho_l^0\right)/2$ (subscript l denotes the lower layer properties). Upon initiation of grid oscillations, turbulence quickly fills the homogenous layer between the two interfaces.

It is common to represent oscillating-grid turbulence by the so-called grid "action" parameter K introduced by Long [44] as

$$K = uz, \tag{1}$$

where u is the characteristic *rms* velocity at a distance z from the grid (with z modified to include a virtual origin, by adding z_0). The turbulent front generated by each grid propagates in the homogeneous region according to Dickinson and Long [45],

$$r = \alpha(Kt)^{\frac{1}{2}}, \tag{2}$$

where r is the distance from the grid at time t and $\alpha = 0.67$ ([46]; their Fig. 26). Initially, turbulent fronts propagating toward each other merge and form a region of uniform turbulent intensity u_H of thickness ~ $\pm 2L_H$ surrounding the center [39]. Here L_H is the local integral length scale.

On the other hand, turbulent fronts propagating toward and interacting with two density interfaces cause turbulent mixing and entrainment, but the entrainment/migration rate therein is much slower, given the stronger [initial] interfacial buoyancy jumps. For the upper interface this jump is $\Delta b_u^0(t=0) = b_u^0 - b_u(t=0) = \Delta b_0/2$, where $\Delta b_0 = -g(\rho_u^0 - \rho_l^0)/\rho_0$ is the buoyancy jump between the upper and lower layers. Similarly, $\Delta b_l^0(t=0) = b_l^0 - b_l(t=0) = \Delta b_0/2$. Below we discuss anticipated processes at the upper interface, noting that a similar description also applies to the lower interface.

Following local mixing of entrained lighter fluid from aloft with that below the interface, the mixed fluid propagates downward according to Eq. (2), $y_1 = \alpha\left(Kt'\right)^{1/2}$, where y_1 is the distance traveled by the front over time t' ($t' \approx t$). This rapid propagation is possible because of meager buoyancy effects at the mixed front, unlike at the initial density interface proper. The region behind the front is assumed to be quasi homogeneous, and its density (and b_u) decreases with entrainment, thus increasing $\Delta b_u^0(t)$. The rate of mixing and entrainment at stable interfaces have been studied extensively [15], and the normalized

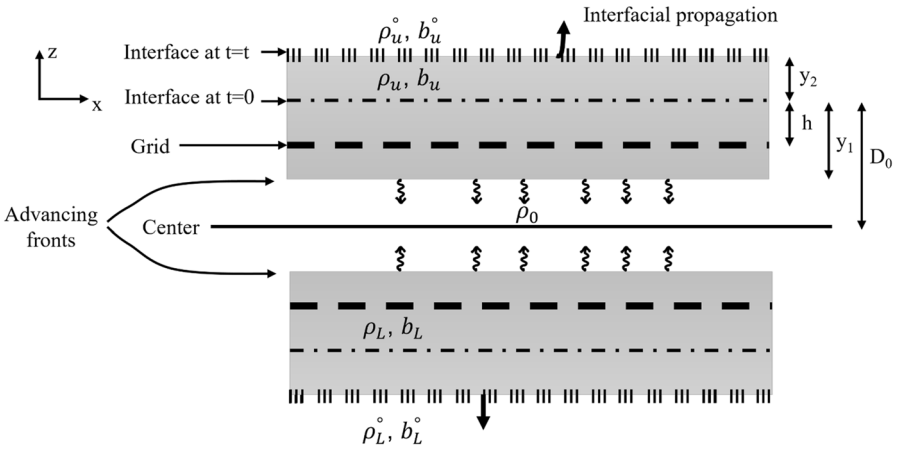

Fig. 5 A schematic of the proposed density-step formation mechanism. Two density interfaces are located above and below [oscillating] grids in a three-layer fluid (see Fig. 4). Local interfacial mixing and entrainment at each interface produce mixed fluid, which diffuses toward the center [of the middle layer] as fronts with disparate densities under background grid turbulence. The fronts meet at the center, where a density step may form under favorable conditions

entrainment rate is expressed in terms of the well-known Richardson number power law [15, 28]

$$\frac{u_e}{u_i} = \frac{1}{u_i}\frac{dy_2}{dt} = \alpha_1 Ri^{-n}, \tag{3}$$

where y_2 is the migrating interfacial position, n (>0) an entrainment exponent, α_1 denotes a constant, and $Ri_0 = \Delta b_u^o (y_2 + h)^3 / K^2$ a bulk Richardson number based on the interfacial buoyancy jump $\Delta b_u^o(t)$, distance to the interface from the grid $(y_2 + h)$, and *rms* turbulent velocity at the interface $u_i = K/(y_2 + h)$ (Fig. 5). The buoyancy flux at the upper interface can be calculated using the buoyancy conservation equation by assuming a density interface of negligible thickness as

$$q_u = -\overline{b'w'} = \Delta b_u^0 \frac{\partial y_2}{\partial t}, \tag{4}$$

where $\Delta b_u^0 = b_u^0 - b_u = -g(\rho_u^0 - \rho_u)/\rho_0$. Similarly, integration of buoyancy conservation equation over the growing layer $-y_1(t) < \zeta < y_2(t)$ becomes

$$-(y_1 + y_2)\frac{\partial b_u}{\partial t} = (y_1 + y_2)\frac{\partial \Delta b_u^0}{\partial t} = -q_u. \tag{5}$$

Combining Eqs. (4) and (5) gives,

$$(y_1 + y_2)\frac{\partial b_u}{\partial t} = -(y_1 + y_2)\frac{\partial \Delta b_u^0}{\partial t} = \Delta b_u^0 \frac{\partial y_2}{\partial t} \tag{6}$$

Assuming symmetry, similar equations can be obtained for the lower interface, viz.,

$$q_l = -\overline{b'w'} = \Delta b_l^0 \frac{\partial y_2}{\partial t} \tag{7}$$

and

$$\left(y_1 + y_2\right)\frac{\partial b_l}{\partial t} = \left(y_1 + y_2\right)\frac{\partial \Delta b_l^0}{\partial t} = -\Delta b_l^0 \frac{\partial y_2}{\partial t}. \tag{8}$$

Thus, the buoyancy difference $\Delta b = b_u - b_l$ between the downward and upward propagating fronts evolve according Eqs. (5)–(8) as

$$\left(y_1 + y_2\right)\frac{\partial(\Delta b)}{\partial t} = \left(\Delta b_0 - \Delta b\right)\frac{\partial y_2}{\partial t}. \tag{9}$$

The entrained fluid from the upper and lower layers into the middle layers is distributed in the turbulent region behind the front. When the fronts meet, they attempt to penetrate past each other only to be retarded by the buoyancy difference Δb in the center area.

Considering the rapid growth of y_1 compared to y_2, Eq. (9) can be integrated from the origin of turbulent fronts to their meeting at $y_1 = D_0$ as

$$\Delta b \approx \Delta b_0 \left(y_2 / y_1\right) \tag{10}$$

The entrainment rate [Eq. (3)] can be rewritten using Eq. (1) for the upper layer as

$$\frac{dy_2}{dt} = \alpha_1 \left(\frac{K}{h + y_2}\right)\left\{\frac{\Delta b_u (h + y_2)^3}{K^2}\right\}^{-n}, \tag{11}$$

where Δb_u is the interfacial buoyancy jump which, for small times, becomes

$$\Delta b_u = \frac{\Delta b_0}{2}\left(1 - \frac{\Delta b}{\Delta b_0}\right), \tag{12}$$

suggesting that the initial Richardson number $Ri_0 = \Delta b_0 h^3 / 2K^2$ is a useful indicator of mixing at the initial phase of flow evolution. Considering $\Delta b \ll \Delta b_0$ and $y_2 \ll h$, and the time scale for the meeting of two fronts

$$t = \frac{D^2}{\alpha^2 K}, \tag{13}$$

it is possible to evaluate

$$y_2 \approx \frac{\alpha_1}{\alpha^2}\left(\frac{D_0^2}{h}\right)\left(Ri_0^{-n}\right) \tag{14a}$$

and

$$\Delta b \approx \frac{\alpha_1}{\alpha^2}\frac{\Delta b_0 D_0}{h} Ri_0^{-n}. \tag{14b}$$

The proposed criterion in Sect. 5 for the step structure formation can now be applied as

$$\frac{\Delta b L_H}{u_H^2} > Ri_c,$$
$$\frac{\alpha_1}{\alpha^2}\left[\frac{\Delta b_0 L_H}{u_H^2}\right]\frac{D_0}{h}Ri_0^{-n} > Ri_c, \text{ or} \tag{15}$$
$$I = \left[\frac{\Delta b_0 L_H}{u_H^2}\right]\frac{D_0}{h}Ri_0^{-n} > Ri_c\frac{\alpha^2}{\alpha_1}$$

Thus, I is a crucial parameter governing the formation of density steps in present experiments. It helps avoid the measurement of Δb, which is very difficult to measure at the time of the step formation.

8 Evaluation of relevant parameters during experiments

According to Eq. (15), the [measurable] parameter I is the sole governing parameter for the problem, and the formation of a density step during experiments requires $I > Ri_c\alpha^2/\alpha_1$. During initial filling, some mixing between the layers was unavoidable, thus the initial interface was somewhat diffused, and the interface was sharpened by suction of a small amount of fluid from the middle of the interface. The initial interfacial thickness was $\leq$ 0.3 cm, and hence could assumed to be negligible. In calculating I, the required Δb_0, D_0 and h were determined from the initial density profile. The locations of the upper edge of the middle layer and lower edge of the upper layer were obtained using the intersection of the tangent to the density profile $\rho(z)$ at the [thin] interfacial midpoint $\rho_m = \left(\rho_u^0 + \rho_0\right)/2$ with the surrounding densities. The same method was adopted for the lower layer. In applying this method for a migrating interface, it was necessary to smooth the density profiles to remove the raggedness of the profiles introduced by small-scale inversions. The smoothing was conducted using the Thorpe ordering procedure discussed in De Silva and Fernando [40].

According to Eq. (15), the length scale L_H and the rms horizontal velocity u_H at the step formation (central) region are necessary to calculate I. As mentioned, oscillating-grid turbulence studies, which are extensive (see Kit et al. [47] and references therein), have shown that for a single grid these quantities vary as

$$L_H = c_1\xi \quad u_H = c_2 fM^{1/2}S^{3/2}\xi^{-1} \quad \text{so that } K = c_2 fM^{1/2}S^{3/2} \tag{16}$$

where ξ is the distance from the grid mid plane [with an adjustment for a virtual origin located at a distance $(S/2 \pm 1$ cm)], S the stroke of grid oscillations, M the grid mesh size and the constants are $c_1 \approx 0.10$ and $c_2 \approx 0.25$ for the present case [48]. Srdic et al. [39] have shown that velocity and length scales of turbulence for the double-grid case (Fig. 4) can also be approximately given by Eq. (16), with the same c_1 and a higher c_2. Thus u_H, L_H and K at the center for the double-grid case were evaluated using Eq. (16) with $\xi_c = D_0 - h + 1cm$ after correcting for the virtual origin. Turbulence intensity at the center was evaluated considering the cumulative effect of two turbulence sources (grids) as $u_H = \sqrt{2}c_2 fM^{1/2}S^{3/2}{\xi_c}^{-1}$.

To complete the calculation of I, the value of n is necessary, which has been measured in numerous occasions for single and double grid experiments for sharp interfaces [15]. In the present case, however, the step formation occurs within the first few minutes of

interfacial mixing, and hence n is expected to be appreciably different from that observed in previous experiments, i.e., $n = 1.2$—1.75. To address this issue, the rate of entrainment for the first three minutes was measured in several separate experiments as a function of Ri_0, and an average value of $n \approx 0.5 \pm 0.12$ was observed, which was used to calculate I in Eq. (15). This value is consistent with the low Ri asymptote reported by Christodulou [49] for entrainment experiments. At the initiation of experiments, the diffused nature of the interface despite efforts to generate a sharp interface and a transient evolution of interface tends to yield a different entrainment law.

9 Experimental observations

After a series of successful pilot experiments to investigate the feasibility of the proposed mechanism, ten systematic experiments were performed to determine the critical value of I above which the density step is formed. These experiments are listed in Table 2. Because of the difficulty of fine-controlling the stratification as well as layer locations and their thicknesses, regular increments of I could not be pursued. The criteria used to identify the appearance of a density step was that, during the observational period, a sharp density jump of $> 10\%$ appears at the central portion ($\pm 0.2\ Do$) of the middle layer, corroborated by qualitative shadowgraph observations.

Figure 6 shows a set of density profiles taken at $t = 0$, 3 and 5 min following the initiation of two experiments with $I = 1.53$ and 1.75. Note the distinct density step in the latter case and no identifiable interface in the former. All experiments with $I < 1.53$ did not show the formation of a density step and experiments with $I > 1.75$ showed a density step in the center region within the first three minutes. This observation together with the other experiments listed in Table 3 show that the critical value of I for the formation or non-formation of steps lies in the range $1.53 < I < 1.75$. The estimated accuracy for the determination of I is $\sim \pm 10\%$. Taking reported values of $\alpha = 0.67$ [45] and based on current experiments $\alpha_1 = 0.41$, the local Richardson numbers $Ri = \Delta b L_H / u_H^2$ could be reckoned using Δb from Eq. (14b) as well as L_H and u_H using the discussion following Eq. (16). These Ri values are listed in Table 2, from which Ri_c was found to be in the range $1.36 < Ri_c < 1.56$. In all, it is possible to infer that $Ri_c \approx 1.5$.

10 Conclusions and discussion

The aim of this paper was to present observations of step like microstructure formation in the lower marine ABL in the presence of fog, and present a possible mechanism of step formation in the fog-laden ABL. Such conditions are profusely unfavorable for electro-optic propagation, and hence a study of conditions of their genesis is opportune. It was argued that density steps are possible during localized turbulent mixing events in stably stratified fluids, wherein initial downward turbulent diffusion of lighter fluid parcels as a front and upward turbulent diffusion of heavier fluid parcels likewise may not pass each other during the initial osculation if the buoyancy jump Δb across the fronts are stronger than inertial forces of turbulent eddies u_H^2/L_H, where L_H and u_H are the integral length and velocity scales, respectively, in the area of step formation. Thus, the criteria for the step formation can be written as $Ri = \Delta b L_H / u_H^2 > Ri_c$, where Ri_c is a critical Richardson number.

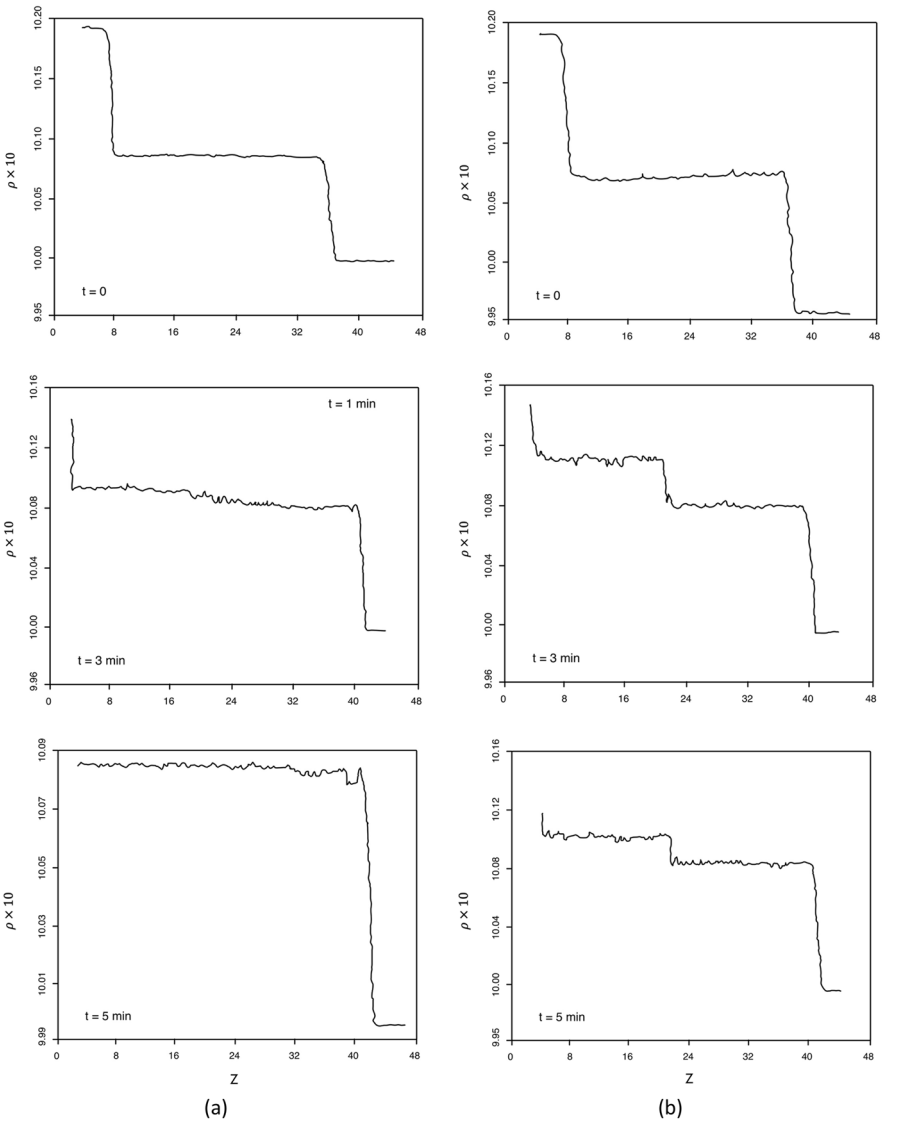

Fig. 6 Representative density (ρ, in g cm^{-3}) profiles from two experiments **a** without interfacial layer formation ($I = 1.53$) and **b** with interfacial layer formation ($I = 1.75$). Here z is measured from an arbitrary location in the upper layer

A simple laboratory experiment was performed to demonstrate the efficacy of the proposed mechanism, notwithstanding the challenge of working with rapidly propagating turbulent fronts that osculate at a region of quasi homogeneous turbulence to produce a buoyancy jump of required strength. Using two oscillating grids in the middle layer of a three-layer stratified fluids, with grids placed at a suitable distance from the interfaces between layers and oscillated symmetrically above and below the center of middle layer, it was possible to obtain counter propagating density fronts initiated due to localized

Table 2 Experimental parameters and the possible formation of an interface. Shading shows experiments that demarcate the conditions of step formation

	Δb_0 cms^{-2}	f Hz	K cm^2s^{-1}	D_0 cm	h cm	ξ_c cm	Ri_0	I	Ri	Density step
1	20.43	5	18.30	13.4	5.5	8.9	8.37	1.53	1.36	No
2	22.40	5	18.30	14.5	5.5	10	9.18	2.46	2.19	Yes
3	22.40	5	18.30	14.5	6.0	9.5	11.47	1.75	1.56	Yes
4	18.50	5	18.30	13.5	6.0	8.5	9.47	1.06	0.94	No
5	18.50	5	18.30	13.0	5.5	8.5	7.58	1.23	1.09	No
6	16.57	5	18.30	13.0	6.0	8	8.48	0.80	0.71	No
7	16.57	4	14.64	13.5	6.0	8.5	13.26	1.25	1.12	No
8	22.40	4	14.64	14.5	5.5	10	14.35	3.07	2.74	Yes
9	22.40	4	14.64	15.0	5.0	11	11.28	5.17	4.61	Yes
10	20.43	4	14.64	13.5	5.5	9	13.08	1.99	1.78	Yes

turbulent mixing at the two interface and meet at the center part of the middle layer. This region is expected to have approximately spatially uniform turbulence intensities. Oscillating grid turbulence has been studied extensively, and previously reported results immensely helped characterize turbulence. Experiments with varying interfacial jumps and turbulent intensities were conducted, and the buoyancy jump across propagating fronts and their propagating speeds were reckoned using a simple model based on buoyancy conservation equations, entrainment law for stratified interfaces, and properties of oscillating grid turbulence. Measurements and accompanying model calculations indicated a critical Richardson number of $Ri_c \approx 1.5$. The water vapor acts as a passive scalar during the formation of steps, and hence the present results can be applied to cases of density steps with fog.

This result can be applied to the step structure observed in Fig. 2a.iv and v, with Fig. 2a. iii a precursor (preconditioning) to step formation with some mixing activity. Commonly used length scales to characterize such situations are the buoyancy length scale u_H/N and the Ozmidov length-scale $\left(\varepsilon/N^3\right)^{1/2}$, which are listed in Table 3. They are only a fraction of the lower stratified layer, indicating localized mixing. The large value of the Gibson parameter $\varepsilon/\nu N^2$ indicates active three-dimensional turbulence and mixing.

The second row of Table 3 lists the bow-mast measured turbulence quantities at the height 12.5 m, the buoyancy jump Δb across the lowest step and the Richardson number Ri. The calculated Ri is larger than Ri_c, showing consistency with the proposed criterion. Here L_H was calculated using the autocorrelation function method and u_H using 15 min averaging. The third row shows conditions at 02:19 UTC (Fig. 2a.v), where continuation of layered structure is evident, which is consistent with $Ri > Ri_c$. In summary, the results point to the formation of density steps during initial evolution of a stratified turbulent region when $\Delta b L_H/u_H^2 > Ri_c$. Also, field observations suggest mixing fog appearance during the turbulence event.

Finally, it is interesting to note several other atmospheric and oceanic examples of step or staircase formation in stratified regions by the mechanism described here, in particular by Kelvin Helmholtz (KH) billowing induced by local shear instabilities. When KH billowing occurs, strong turbulence is generated locally in the 'eye' of the billow from the very early stages of evolution [50]. The overturning motions cause a turbulent mixing layer bounded by interfaces, and entrainment at their edges cause lighter and denser fluid parcels to osculate within the mixing region, all the while turbulence is undergoing decay due to weakening shear. It is possible to expect layer formation within the mixing layer if $\Delta b L_H/u_H^2 > Ri_c$. A

Table 3 observed and calculated parameters at times of field rawinsondes

Start time (15 min trace)	ABL conditions	Observed parameters	Calculated parameters
09/12/2018 23:11 UTC (Fig. 2a.iii)	No layering; linear θ_E profile at surface level; onset of visibility reduction	Lower layer $N \approx 0.026$ rad/s (rawinsonde data up to 100 m); surface $u_H \approx 0.37$ m s^{-1}, $L_H = 110$ m, $\varepsilon \approx 0.02$ m^2 s^{-3} (bow mast); thickness of lower stratified layer $\approx$ 100 m	Buoyancy length scale $u_H/N \approx$ 14.3 m; Ozmidov scale $\left(\varepsilon/N^3\right)^{1/2} \approx 34$ m $\varepsilon/\nu N^2 \approx 5\times10^6$ (Active turbulence)
09/13/2018 01:00 UTC (Fig. 2a.iv)	Layered structure (density steps) appears; low visibility with fog; weak shear and low wind speeds	Across the steps $\Delta b = 0.03$ ms^{-2}; lower layer $L_H = 11.5$ m and $u_H = 0.38$ m s^{-1}; $\varepsilon \approx 0.02$ m^2 s^{-3} (based on bow mast sonic)	At the interface $Ri = \frac{\Delta b L_H}{u_H^2} \approx 2.4$ ($> Ri_c$; recently formed steps)
09/13/2018 02:19 UTC (Fig. 2a.v)	Layered structure present and upper layer evolving; fog; weak shear and low wind speeds	Across the step $\Delta b = 0.05$ m s^{-2}; lower layer $L_H = 72$ m and $u_H = 1$ m s^{-1}; $\varepsilon \approx 0.05$ m^{2}s^{-3} (based on bow mast sonic)	$Ri = \frac{\Delta b L_H}{u_H^2} \approx 3.6$ ($> Ri_c$; interface is viable)

middle-atmospheric example of such mixing is shown in Fig. 7a from Luce et al. [51] where observations from high frequency Middle and Upper atmosphere Radar (MUR) are shown, taken 08 October 2008. Note the maturation of a KH billowing event at ~ 04:03 Local Time (LT), with the thickness of the mixing layer ~ 1 km. A growing mixing layer (green color) appears separated by upper and lower interfaces. At 04:03 LT, buoyancy jump across the middle mixing layer is ~ 0.14 m s^{-2}, $L_H \approx 50$ m and $u_H^2 \approx 5$ m^2 s^{-2} (see Fig. 7 caption for details), yielding $Ri = \Delta b L_H / u_H^2 \approx 1.4$. No interface can be noted, consistent with the Ri_c criterion. At

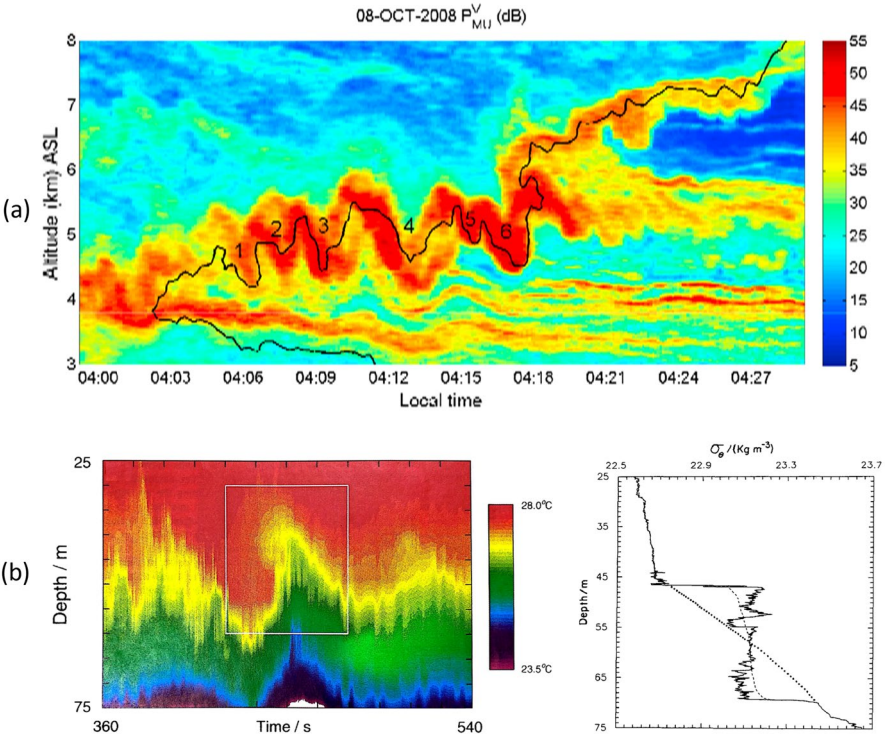

Fig. 7 **a** A Kelvin Helmholtz (KH) billow observed by very high frequency Middle and Upper atmosphere Radars (MUR) by Luce et al. [51]. Radar echoes (dB) corrected for the range attenuation are shown on a time-height cross section. Radiosondes launched at representative sites show the breakdown of KH billows ~ 04:00 LT (their Fig. 3 lower) and development of approximately mixed patches of thickness ~ 1.0 km at about 04:02 LT (their Fig. 2) at the level of the billows with an estimated buoyancy jump of $\Delta b \approx 0.14$ m s^{-2}, the rms turbulent velocity scale $u_H^2 \approx 5$ m^2 s^{-2} [51]. $L_H \approx 50$ m can be evaluated as 1/20 of the patch size ([40], Sect. 5). A mixing layer forms between the two interfaces generated by billowing, and no steps are formed in the mixing layer at first. Upper interface again becomes unstable, and protuberances generated by billows are numbered and are discussed in Luce et al. [51]. Decay of turbulence ensued in the mixed layer and a density step appears at 04:12 LT, when the mixing layer thickness ~ 0.75 km ($L_H \approx 37.5$ m) and $u_H^2 \approx 3$ m^2 s^{-2} [51]. **b** Possible breaking of a KH billow in the equatorial undercurrent and associated formation of a turbulent patch of thickness 22.6 m as reported in Table 1 of Hebert et al. [52] and further analyzed by De Silva et al. [50]. Left figure is the temperature structure presented using Hebert et al. [52] towed thermistor data by De Silva et al. [50] with the white box showing the time frame where a microstructure profiler registered the density structure shown to the right. The buoyancy variability within the patch $\Delta b \approx 2.26 \times 10^{-3}$ m s^{-2} based on buoyancy frequency evaluated using the gradients just inside the patch (their Table 1). Calculations in the text assumes $L_H \approx 1.1$ m to be 1/20 of the patch size and Strang and Fernando [53] result for stratified shear layer rms velocity of $u_H \approx 0.12 \Delta U \approx 0.12$ m s^{-1} (their Sect. 9), where the characteristic shear layer velocity jump is $\Delta U \approx 1$ m s^{-1} [50]

04:12 LT, a step appears in the mixing layer in between the two interfaces formed by billowing, whence the turbulence intensity has reduced to ~ 3 $m^2\ s^{-2}$ (see legend). If buoyancy jump across the mixing layer just before the formation of the step remains ~ 0.14 m s^{-2} and using the thickness of the mixing layer 0.75 km ($L_H \approx 37.5m$), it is possible to obtain $Ri = \Delta b L_H / u_H^2 \approx 1.75$, satisfying conditions for the step formation. The upper interface formed at ~ 04:02 LT undergoes further KH billowing due to local shear at ~ 04:18 LT. The ensuing mixed layer leads to an interface at ~ 04:22 LT, and successive breakdowns are expected to yield multiple layering and a density staircase.

An oceanic example of a K-H billow observed by Hebert et al. [52] is shown in Fig. 7b, where billow breakdown generated a turbulence patch, the properties of which were studied by De Silva et al. [50]. As indicated in the figure caption, the estimated values for the patch are $\Delta b \approx 2.26 \times 10^{-3}$ m s^{-2}, $u_H \approx 0.12$ m s^{-1} and $L_H \approx 1.13$ m, yielding $Ri = \Delta b L_H / u_H^2 \approx 0.18 < Ri_c$. This is consistent with the absence of a well-defined step like structure within the patch.

Acknowledgements We thank the science and marine crew of the R/V Hugh R. Sharp and Earnest Knoors and Mark van de Zende for helping with the initial laboratory experiments. Over the years the first author and his students and post-docs collaborated with Professor Peter A. Davies, via which they have greatly benefited. Some of the joint work included oscillating grid turbulence in stratified and rotating fluids. In commemoration of this productive collaboration, we are honored to be able to contribute to this special issue of EFM.

Author Contributions HJSF wrote the main manuscript text and integrated different components. SW acquired and analyzed the field data and prepared Figs. 1 and 2. KYH performed calculations on the lab experiment data, helped with illustrations and prepared Figs. 4 and 7. EC was the chief scientist of the cruise and coordinated field data acquisition. All authors reviewed and revised the manuscript.

Funding This work was supported by the Grants # N00014-21-1-2296 (Fatima Multidisciplinary University Research Initiative MURI) and # N00014-18-1-2472 (Toward Improving Coastal Fog Prediction C-FOG) of the Office of Naval Research, administered by the Marine Meteorology and Space Program.

Declarations

Conflict of interest The authors declare that they have no conflict of interest to disclose.

References

1. Li X, Gaynor JE, Kaimal JC (1983a) Studies of nocturnal stable layers at BAO. In: Kaimal JC (ed) NOAA Boulder atmospheric Observatory Rep #4 January, pp 75–90
2. Li X, Gaynor JE, Kaimal JC (1983) A study of multiple stable layers in the nocturnal lower atmosphere. Boundary-Layer Meteorol 26(2):157–168
3. Glazunov AV, Mortikov EV, Barskov KV, Kadantsev EV, Zilitinkevich SS (2019) Layered structure of stably stratified turbulent shear flows. Izves Atmos Ocean Phys 55(4):312–323
4. Fernando HJS (1988) The growth of a turbulent patch in a stratified fluid. J Fluid Mech 190:55–70
5. Wang K, Wang M (2012) Aero-optics of subsonic turbulent boundary layers. J Fluid Mech 696:122–151
6. Geernaert GL (2007) On the evaporation duct for inhomogeneous conditions in coastal regions. J Appl Meteorol Climatol 46(4):538–543
7. Harris D (1995) The attenuation of electromagnetic waves due to atmospheric fog. Int J Infrared Millim 16(6):1091–1108
8. Torregrosa A, O'Brien TA, Faloon IC (2014) Coastal fog, climate change, and the environment. Eos Trans AGU 95(50):473–474
9. Fernando HJS, Gultepe I, Dorman C, Pardyjak E, Wang Q, Hoch S, Richter D, Creegan E, Gabersek S, Bullock T, Hocut C, Chang R, Alappattu D, Dimitrova R, Flagg D, Grachev A, Krishnamurthy R,

Singh DK, Lozovatsky I, Nagare B, Sharma A, Wagh S, Wainwright C, Wroblewski M, Yamaguchi R, Bardoel S, Coppersmith R, Chisholm N, Gonzalez E, Gunawardena N, Hyde O, Morrison T, Olson A, Perelet A, Perrie W, Wang S, Wauer B (2021) C-FOG: life of coastal fog. Bull Am Meteorol Soc 102(2):E244–E272
10. Dorman CE, Grachev AA, Gultepe I, Fernando HJS (2021) Toward improving coastal-fog prediction (C-FOG). Boundary-Layer Meteor 181(2):167–170
11. Wang S, Fernando HJS, Creegan E, Krishnamurthy R, Wainwright C, Wagh S (2021) Analysis of a coastal marine fog episode during C-FOG. Boundary-Layer Meteor 18:365–393
12. Wagh SD, Krishnamurthy R, Wainwright C, Wang S, Dorman C, Fernando HJS, Gultepe I (2021) Microphysics of marine fog formed by stratus lowering. Boundary-Layer Meteor 181:317–344. https://doi.org/10.1007/s10546-021-00670-w
13. Bolton D (1980) The computation of equivalent potential temperature. Mon Weather Rev 108:1046–1053
14. May RM, Arms SC, Marsh P, Bruning E, Leeman JR, Goebbert K, Thielen JE, Bruick ZS (2022) MetPy: a python package for meteorological data. https://github.com/Unidata/MetPy
15. Fernando HJS (1991) Turbulent mixing in stratified fluids. Ann Rev Fluid Mech 23:455–493
16. Fernando HJS (1995) Migration of density interfaces subjected to differential turbulent forcing. J Geophys Astrophys Fluid Dyn 78:1–20
17. Woods JD (1968) Wave induced shear instability in summer thermocline. J Fluid Mech 32:791–800
18. Padman L, Dillon TM (1987) Vertical fluxes through the Beaufort Sea thermohaline staircases. J Geophys Res 92:10799–10806
19. Ruddick B, McDougall TJ, Turner JS (1989) The formation of layers in a uniformly stirred density gradient. Deep-Sea Res 36(4):597–609
20. Zatsepin AG, Gerasimov VV (2022) Turbulent mass exchange in a stratified fluid and the conditions of Its fine structure layering. Physical and mathematical modeling of earth and environment processes. Springer, Cham, pp 219–230
21. Holford JM, Linden PF (1999) Turbulent mixing in a stratified fluid. Dyn Atmos Oceans 30(2–4):173–198
22. Balmforth NJ, Smith SGL, Young WR (1998) Dynamics of interfaces and layers in a stratified turbulent fluid. J Fluid Mech 355:329–358
23. Wunsch S, Kerstein A (2001) A model for layer formation in stably stratified turbulence. Phys Fluids 13(3):702–712
24. Dillon TM (1982) Vertical overturns: a comparison of Thorpe and Ozmidov length scales. J Geophys Res 87:9601–9613
25. Phillips OM (1971) On spectra measured in an undulating layered medium. J Phys Oceanogr 1(1):1–6
26. Garret C, Munk W (1972) Space-time scales of internal waves. Geophys Fluid Dyn 3:225–264
27. Turner JS, Stommel H (1964) A new case of convection in the presence of vertical salinity and temperature gradients. Proc Natl Acad Sci 52:49–53
28. Turner JS (1973) Buoyancy effects in fluids. Cambridge University Press
29. Huppert HE, Turner JS (1981) Double-diffusive convection. J Fluid Mech 106:299–329
30. Ivey GN, Corcos GM (1982) Boundary mixing in a stratified fluid. J Fluid Mech 121:1–26
31. Brown JM, Radko T (2019) Initiation of diffusive layering by time-dependent shear. J Fluid Mech 858:588–608
32. Phillips OM (1972) Turbulence in a strongly stratified fluid—is it unstable? Deep Sea Res and Oceanogr Abs 19(1):79–81
33. Posmentier ES (1977) The generation of salinity fine structure by vertical diffusion. J Phys Oceanogr 7:292–300
34. Baranblatt GI, Bertsch M, Passo RD, Prostokishin VM, Ughi M (1993) A mathematical model of turbulent heat and mass transfer in stably stratified shear flow. J Fluid Mech 253:341–358
35. Noh Y, Fernando HJS (1991) A numerical study on the formation of a thermocline in shear-free turbulence. Phys Fluids A 3(3):422–426
36. Linden PF (1979) Mixing in stratified fluids. J Geophys Astrophys Fluid Dyn 13(1):3–23
37. Fernando HJS, Hunt JCR (1996) Some aspects of turbulence and mixing in stably stratified layers. Dyn Atmos Ocean 23:55–61
38. Taylor GI (1917) The formation of fog and mist. Q J R Meteorol Soc 43:241–268
39. Srdic A, Fernando HJS, Montenegro L (1996) Generation of nearly isotropic turbulence using two oscillating grids. Exp Fluids 20(5):395–397
40. De Silva IPD, Fernando HJS (1992) Some aspects on mixing in stratified turbulent patches. J Fluid Mech 240:601–625

41. De Silva IPD, Fernando HJS (1994) Oscillating grids as a source of nearly isotropic turbulence. Phys Fluids 6(7):2455–2464
42. Mcdougall TJ (1979) Measurements of turbulence in a zero-mean-shear mixed layer. J Fluid Mech 94(3):409–431
43. Fernando HJS, De Silva IPD (1993) Note on secondary flows in oscillating-grid mixing box experiments. Phys Fluids A 5(7):1849–1851
44. Long RR (1978) Theory of turbulence in a homogeneous fluid induced by an oscillating grid. Phys Fluids 21(10):1887–1888
45. Dickinson SC, Long RR (1983) Oscillating grid turbulence including the effects of rotation. J Fluid Mech 126:315–333
46. Fernando HJS, Long RR (1985) On the nature of the entrainment interface of a two-layer fluid subjected to zero-mean-shear turbulence. J Fluid Mech 151:21–53
47. Kit ELG, Strang EJ, Fernando HJS (1997) Measurement of turbulence near shear-free density interfaces. J Fluid Mech 334:293–314
48. Hopfinger EJ, Toly JA (1976) Spatially decaying turbulence and its relation to mixing across density interfaces. J Fluid Mech 78:155–175
49. Christodoulou GC (1986) Interfacial mixing in stratified flows. J Hydraul Res 24(2):77–92
50. De Silva IPD, Fernando HJS, Eaton F, Hebert D (1996) Kelvin-Helmholtz billows in nature and laboratory. Earth Planet Sci Lett 143(1–4):217–231
51. Luce H, Mega T, Yamamoto MK, Yamamoto M, Hashiguchi H, Fukao S, Nishi N, Tajiri T, Nakazato M (2010) Observations of Kelvin-Helmholtz instability at a cloud base with the middle and upper atmosphere (MU) and weather radars. J Geophys Res Atmos 115:D19116
52. Hebert D, Moum JN, Paulson CA, Caldwell DR (1992) Turbulence and internal waves at the equator. Part II: details of a single event. J Phys Oceanogr 22:1346–1356
53. Strang EJ, Fernando HJS (2001) Entrainment and mixing in stratified shear flows. J Fluid Mech 428:349–386